NANO LETTERS

Letter

pubs.acs.org/NanoLett

Engineering Graphene Mechanical Systems

Maxim K. Zalalutdinov,[†] Jeremy T. Robinson,*[,†] Chad E. Junkermeier,[‡] James C. Culbertson, Thomas L. Reinecke, Rory Stine,[§] Paul E. Sheehan, Brian H. Houston, and Eric S. Snow

Naval Research Laboratory, Washington, D.C. 20375, United States

Supporting Information

ABSTRACT: We report a method to introduce direct bonding between graphene platelets that enables the transformation of a multilayer chemically modified graphene (CMG) film from a "paper mache-like" structure into a stiff, high strength material. On the basis of chemical/defect manipulation and recrystallization, this technique allows wide-range engineering of mechanical properties (stiffness, strength, density, and built-in stress) in ultrathin CMG films. A dramatic increase in the Young's modulus (up to 800 GPa) and enhanced strength (sustainable stress ≥1 GPa) due to cross-linking, in combination with high tensile stress, produced high-performance (quality factor of 31 000 at room temperature) radio frequency nanomechanical resonators. The ability to fine-tune intraplatelet mechanical properties through chemical modification and to locally activate direct carbon−carbon bonding within carbon-based nanomaterials will transform these systems into true "materials-by-design" for nanomechanics.

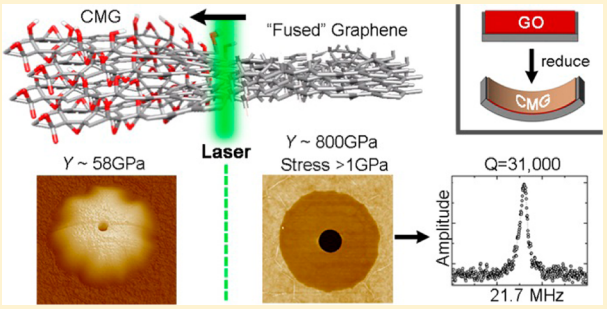

KEYWORDS: *Graphene, cross-linking, quality factor, nanomechanics, resonator, functionalization*

The benefits that carbon-based compounds provide for mechanical systems are best illustrated by ubiquitous carbon-reinforced polymers (CRP).[1] An emblematic composite, light and strong, the CRP comprises high-strength fibers and a filler (e.g., epoxy) required to hold it together. More recently, this "fiber-filler" concept has been extended into graphene systems, where graphene oxide (GO) papers can have ions[2] or polymer chains that hydrogen-bond GO platelets together.[3] Advantageous as they are, these nanocomposites share a weakness with traditional CRP: at critical loads (e.g., shear) the filler becomes the weak link, limiting the composite performance. For nanomechanical systems, it remained a dream that "...stacks of graphene layers could be converted to a product that has a mixture of trivalently and tetravalently bonded carbon atoms — or perhaps only tetravalently bonded, like diamond."[4]

Herein, we report that chemical modification and defect manipulation in chemically modified graphene (CMG) films enabled us to engineer bonding both within the sheets (in-plane) and between the sheets (out-of-plane). Most dramatically, the appropriate application of these treatments can "activate" flakes within a CMG film such that thermal excitation induces direct carbon−carbon bonding between layers. Notably, it is the absence of conventional fillers that enables closer proximity of neighboring graphene planes, where interplatelet bonding can be activated and increase the Young's modulus to ∼800 GPa (close to ∼1 TPa of pristine graphene[5,6] or diamond; in contrast to ∼60 GPa for graphene composites). We view this "direct fuse" paradigm being readily expandable to other carbon-based systems, including carbon nanotubes (CNTs) and fullerenes. In total, our results reveal that a properly prepared initial state, together with well-controlled "fusing", can deliver ultrathin carbon films best-tuned for a particular nanomechanical system.

From a materials perspective, the critical variables that define the performance of nanomechanical structures include strength, stiffness, and built-in stress. In particular, stress engineering can enhance the quality factor (Q) of nanomechanical resonators by orders-of-magnitude,[7] leading to improved mass sensitivity or frequency selectivity. In contrast to conventional microelectromechanical (MEMS) materials (e.g., Si, SiN, etc.), the all-surface nature of graphene provides unprecedented access to and control of its intrinsic properties even after deposition. Since all atoms in graphene are surface atoms, the addition and removal of adsorbates has a profound impact on lattice spacing and bond stiffness. Control over both stress and stiffness at the intraplatelet level, combined with a tunable extent of cross-linking (interplatelet mechanics), are unique for graphene and can provide a degree of freedom unavailable in traditional NEMS materials.

To characterize such behaviors, we start with the evolution of in-plane (intraplatelet) tensile stress engineered in graphene films by different atomic adsorbates through combining numerical analysis based on density-functional theory (DFT) and wafer-bending measurements. While important as a stress tuning mechanism, the cycle of oxidation, fluorination, and reduction is also instrumental in creating defects that prime

Received: May 13, 2012
Revised: June 22, 2012
Published: July 5, 2012

ACS Publications © 2012 American Chemical Society

CMG into a fusable state. The profound effect that interplatelet cross-links impose on mechanical properties of CMG is demonstrated through the behavior of nanomechanical resonators such as domes and cantilevers fabricated in ultrathin CMG films. The analysis of the resonator response allowed us to extract the effect of both chemical modification and cross-link formation on material stiffness (Young's modulus, Y), in-plane stress, and provide a lower bound for film strength.

The rich and tunable chemistry of GO[8] makes it an ideal material with which to study the impact of chemistry on mechanics. Covalent bonding to graphene rehybridizes the carbon bonds from sp^2 to sp^3, modifying its mechanical properties as bond angles shift, distorting the sublattice, and carbon−carbon bond lengths change depending on the adatom.[9] Moreover, wafer-scale GO films are readily available[10] and so allowed us to use straightforward wafer-bending[11] techniques to evaluate large-area, in-plane mechanical stress (σ) as a function of CMG stoichiometry. In these experiments, we deposit continuous GO films on top of 4 in., 100 μm thick or 3 in., 50 μm thick double-side polished Si wafers and use 50 mm long scans in a Veeco Dektak 150 Surface profiler to measure the change in the out-of-plane curvature of the wafers after different stages of thermal or chemical treatment. Wafer bowing toward a dome shape (or bowl shape) is induced by an expanding (or contracting) film, respectively and is directly related to the stress in the film through the Stoney equation (see Supporting Information).

Removing oxygen from GO (thermally or chemically) dramatically increases its tensile stress (σ_{max}) to ∼400 MPa (comparable to σ ∼ 200−1000 MPa in high-stress silicon nitride[12]) due to in-plane lattice contraction (Figure 1A−C). Thermal desorption of oxygen was achieved by either (i) annealing at temperatures ranging from 300−675 K (Figure 1B) or (ii) annealing at a constant temperature (450 K, Figure 1C) for varying times. Likewise, we use hydrazine vapor to chemically removal oxygen. Low-temperature treatments remove intercalated water and slightly increase σ[13] (Region I of Figure 1B), while the desorption of epoxide and carboxyl groups starting at ∼425−450 K[14,15] rapidly increase the film's tensile stress (Region II). A further increase in the annealing temperature to 475−675 K does not significantly affect the stress state (Region III), reflecting a balance between stress generated by oxygen desorption and stress relief via interplatelet or film−substrate slippage.[16] Such relaxation is observed with extended annealing of either chemically or thermally reduced films (Figure 1C).

To understand how the in-plane stress and stoichiometry relate to the underlying energetics, we have made DFT calculations[17] for graphene with a range of adsorbates (Supporting Information Figures S5, S6). Figure 1D shows the equilibrium lattice constants obtained by minimizing the total energies of graphene and of graphene with regular arrays of F (C_xF, $\sim 1 < x < 10$) and of hydroxyl and epoxy defects associated with O adsorption (C_xO, $\sim 1.3 < x < 20$; see Supporting Information Figure S5). In all cases the lattice constants decrease with decreasing adsorbate coverage, which results from the transition of sp^3 to sp^2 character in the C−C bonds and the corresponding strengthening of these bonds. To gain insight into the effects of coverage inhomogeneity, calculations were also made for arrays of F and of O related adsorbates arranged into regions of spatially varying densities. The results in Figure 1D and similar calculations for the bulk modulus suggest that the underlying structural and elastic

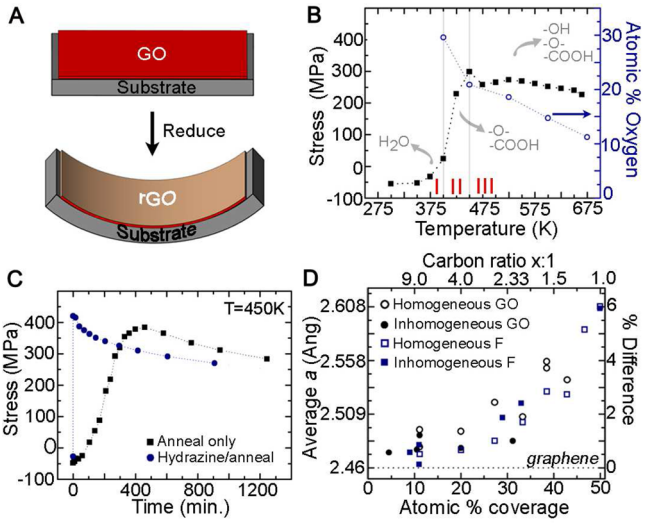

Figure 1. Stress evolution in GO films. (A) Cartoon illustrating a wafer-bending experiment (shown in one direction only). (B) Stress evolution in a GO film (h_o = 40 nm) on a Si wafer (h = 100 μm) during thermal reduction (squares). The stress curve is partitioned into three regions (I, II, III) as labeled at the bottom. Included is oxygen content for a set of samples annealed for 1 h at each temperature (open circles) as measured by X-ray photoelectron spectroscopy (XPS). (C) Stress evolution in an as-deposited GO (black squares) and a hydrazine-reduced GO (blue circles) film versus time (T = 450 K). (D) Plot of calculated average lattice constant (a) versus O or F coverage. The right axis shows the percent deviation from the ideal graphene lattice constant. The top axis shows the atomic carbon ratio for a C_xM_1 material, where M is oxygen or fluorine.

properties are not strongly dependent on inhomogeneity in surface functionalization but rather depend on the average stoichiometry.

An estimate of the highest stress attainable through adatom desorption in C_4O (see Supporting Information Figure S5f), for example, can be made using the calculated change in lattice constant (Figure 1D, strain ∼0.005), which gives a stress of ∼1.3 GPa. The theoretical value for the Young's modulus of C_4O, $Y \approx 259$ GPa, used here assumes defect-free reduction/desorption and a GO sheet thickness of 7.0 Å[18] (see Supporting Information). A combination of factors could produce the lower values of σ measured experimentally (∼400 MPa) including (i) lower film stiffness ($Y \approx 180$ GPa measured for rGO[10]), (ii) not all of the O atoms directly participate in surface functionalization, and (iii) slippage between layers within the film or at the clamping interface.

To experimentally probe the film's local stress (indicative of strength) and stiffness as a function of chemistry, we studied the dynamic response of nanomechanical resonators with variable fluorine coverage. Large arrays of drum resonators (Figure 2A) were fabricated from rGO films (annealed at 450 K; $\sigma_o \approx 400$ MPa; see Figure 1C) using XeF_2 gas etch to remove a silicon sacrificial layer through lithographically defined irrigation holes (Supporting Information Figures S3, S4). The XeF_2 gas serves both to etch the underlying Si and to fluorinate the graphene[19] up to ∼40 atm%, enabling us to measure the impact of fluorine addition.

The in-plane stress in CMG drums (i.e., circular membranes) is calculated using a simple relation between σ and the fundamental resonance frequency (f) given by

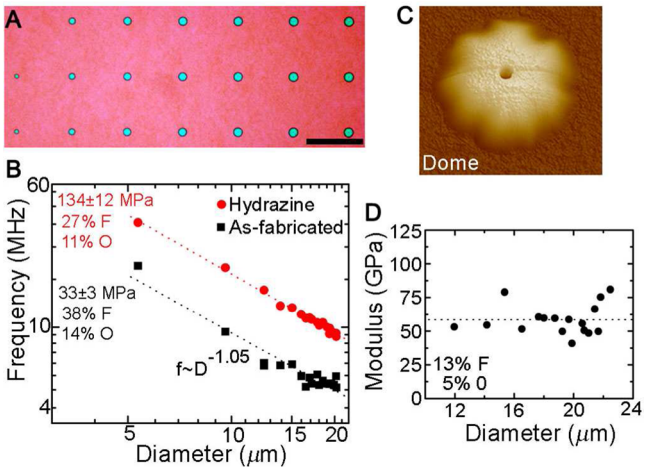

Figure 2. Tuning nanomechanical resonator response. (A) Optical microscope image of as-fabricated resonators (bar = 100 μm). (B) Fundamental resonance frequency versus drum diameter for 18 different drums. The dashed lines are the best-fit power law and the resonator chemistry and stress (eq 1, $\rho = 2.2 \pm 0.2$ g/cm^3) are labeled. Typical variation of f_o for drums of the same diameter is up to ~10%. (C) Perspective AFM image of a relaxed resonator after thermal annealing at 725 K for 1 h ($D \approx 18$ μm, height = 160 nm). (D) Finite element modeling analysis results for the Young's modulus of dome resonators versus dome diameter[10] (see Supporting Information). O and F concentrations were measured by XPS within the surrounding clamped region of the film. The average $\langle Y \rangle = 58.5$ GPa (dotted line in D) with standard deviation of 11 GPa.

$$\sigma = \frac{f^2 D^2}{0.7655}\rho \tag{1}$$

where D is drum diameter and ρ is material density (subject to chemical composition, see Supporting Information). Figure 2B shows the effect of fluorine adsorption/desorption on the fundamental frequency of a series of drum resonators (measured optically[5,10]). Using an estimated film density of $\rho = 2.2 \pm 0.2$ g/cm^3 (see Supporting Information), we find a >10× reduction in stress as the released film expands due to fluorine adsorption, which is consistent with DFT calculations. Desorption of these same fluorine atoms (by ~30%) using hydrazine vapor[19] increased σ approximately 4× ($\sigma \approx 134$ MPa, Figure 2B). This chemically-induced film contraction is consistent with that observed during O desorption in wafer bending experiments (Figure 1B) and confirms the broad applicability of "stoichiometric" stress engineering in different mechanical systems.

While stress tunability based on intraplatelet chemistry is a powerful tool, the interplatelet bonding would be the weak link in the chain and consequently would limit the scope of mechanical applications. To quantify the resilience of our CMG films (i.e., the ability to withstand high tensile stress at elevated temperature) we use stress relaxation experiments[20] based on the negative thermal expansion coefficient (TEC) of graphene ($\alpha_{graphene} \approx -7$ to -2×10^{-6}/K at RT).[16,21] A uniform temperature increase results in a contracting CMG membrane and expanding silicon support frame ($\alpha_{Si} \approx 3 \times 10^{-6}$/K). A 5 min anneal at $T = 725$ K results in complete relaxation (attributed here to interplatelet slippage) and upon cooling to room temperature (RT), the resonator forms a stress-free dome structure (Figure 2C). The formation of wrinkled resonators after annealing between 450 and 600 K is typical for multilayer graphene[21] and rGO,[10] indicating similar interlayer bond strengths in all these systems despite the ranging type and concentration of adsorbates/defects.

These fully relaxed domes have weak interplatelet bonding and resemble paper mache. The stiffness of these CMG films was extracted from the resonant frequency of such wrinkled domes by using the Young's modulus as a fitting parameter in finite element modal analysis[10] (see Supporting Information).

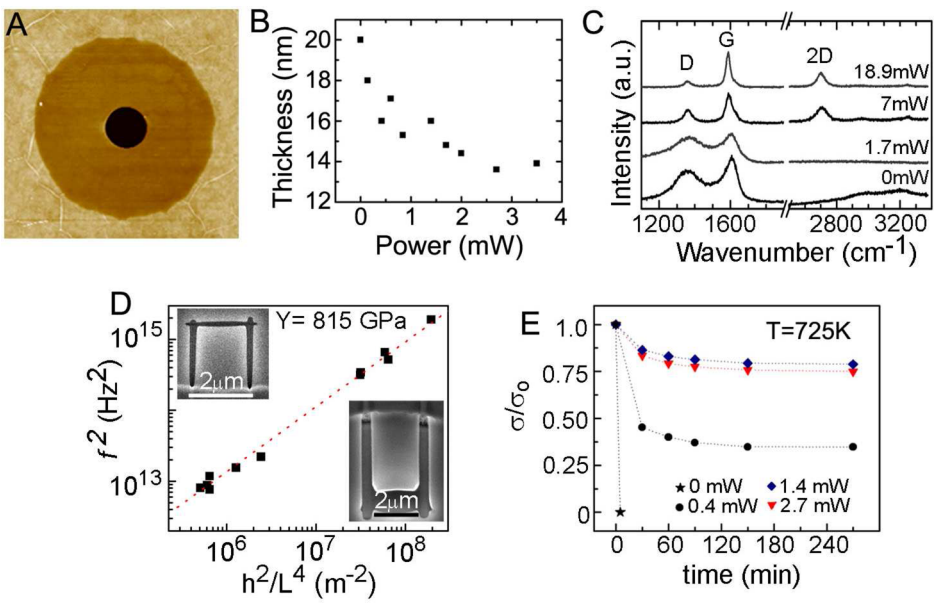

Figure 3. Resonator recrystallization and performance. (A) AFM image of a high-stress drum produced by laser annealing an initially stress-free dome ($D = 17.75$ μm). (B) Resonator thickness versus laser annealing power for neighboring drums. (C) Raman spectra taken from domes thermally reduced at 725 K and subsequently laser-annealed (laser power labeled on right). D) Plot of f^2 versus h^2/L^4 for CMG cantilevers cut from laser-annealed drums ($P_{laser} \approx 1.7$ mW). (inset) SEM images of two cantilevers. (E) Normalized stress ($\sigma/\sigma_o = f^2/f_o^2$) as a function of time for an extended anneal at $T = 725$ K, following laser annealing (laser power labeled).

dx.doi.org/10.1021/nl3018059 | Nano Lett. 2012, 12, 4212−4218

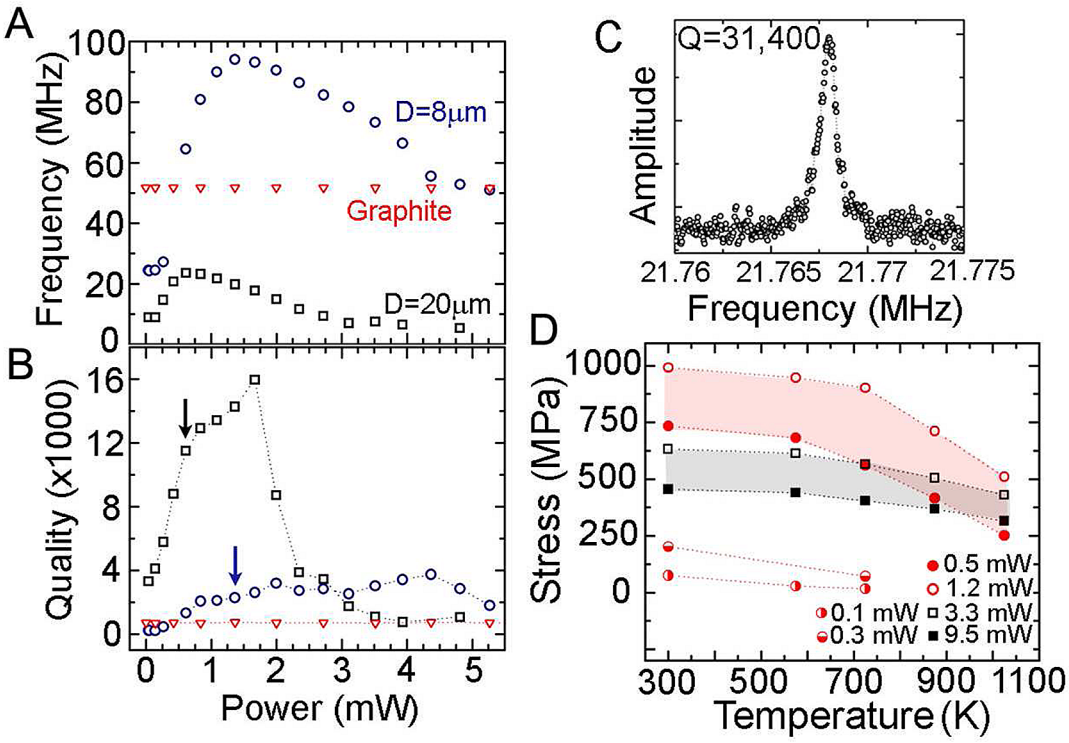

Figure 4. Mechanical properties of recrystallized microstructure. (A,B) Fundamental frequency (f) and quality factor (Q) versus laser annealing power for two CMG dome resonators and one exfoliated graphite resonator ($h_{graphite}$ = 35 nm; D = 6.5 μm). (C) Amplitude-frequency dependence for a laser annealed resonator with Q = 31 400. (D) Residual stress (eq 1, ρ = 2.2 g/cm^3) versus the thermal anneal temperature ($t_{step} \approx 2$ h) for drums initially treated at different laser powers (labeled). Pink band encloses data points for "under-baked" resonators (i.e., with resonance frequency below f_{max}). Gray band highlights the data points for resonators laser-annealed at higher power ($P_{laser} > P(f_{max})$).

On the basis of the fact that the size of the graphene platelets is much smaller than the size of the domes and that the orientation of the flakes is random, our FEM calculations use a transversely isotropic model.[22] The resulting in-plane Young's modulus of $\langle Y \rangle \sim 58$ GPa (standard deviation ≈ 11 GPa; Figure 2D) provides a benchmark for further comparison. Similar values for the in-plane Young's modulus were measured directly in GO papers.[3] DFT calculations (see Supporting Information) confirm that this reduced Young's modulus cannot be explained by residual O or F alone and must be due to weak interlayer coupling and defects left from imperfect reduction. Such defects could be topological, for example, pentagon−heptagon pairs,[23] vacancies, interstitials, or Wigner defects,[24] free radicals or large out-of-plane distortions,[23] leading to regions of quasi-amorphous sp^3 carbon[15,25] or unsaturated bonds.

Remarkably, these remaining defects in the soft film are the starting point for the most dramatic changes in the film mechanics. Highly localized heat (T > 1000 K) produced by laser annealing will recrystallize these defects and cross-link the platelets, thereby inducing desirable high-tensile stresses and enhancing strength and stiffness. Indeed, a few milliwatts of laser power produces a glowing "white-hot" spot within the suspended resonators, while the clamped regions remain cool (see Supporting Information movie). To measure the impact of recrystallization, we laser-annealed stress-free dome resonators with known Y (Figure 2D) and thickness (h).

Exposing these dome-shaped resonators to low-power laser beams (P > 200 μW) causes them to snap flat and to densify, as shown in Figure 3A,B (to be compared to Figure 2C). The rapid change from a relaxed dome to a highly stressed membrane indicates profound structural changes, which we followed with micro-Raman spectroscopy[26] (Figure 3C). Low-power laser annealing (P_{laser} = 1.7 mW) initially broadens the D and G peaks, but higher powers (P_{laser} = 7 mW) narrow the peaks, enhance the G/D ratio, and produce a 2D peak (Figure 3C). Critically, the highest powers (P_{laser} > 18 mW) convert the resonators to virtually defect-free turbostratic graphite, as shown by the vanishing D peak and single-Lorentzian 2D peak (Figure 3C). The increase in resonator density, as well as enhanced sp^2 fraction that accompanies laser annealing, is in line with theoretical analysis that predicts the possibility for low-density disordered carbon to recrystallize at elevated temperature ($T \sim 1000$ K) and to produce a covalently bonded matrix of graphene sheets.[27] Recrystallization both in-plane and out-of-plane is further supported by theoretically predicted structures such as Wigner defects,[24] and by high-resolution transmission electron microscopy (TEM) imaging of irradiated multiwalled CNTs[28] or in-plane "healing" within graphene sheets.[29]

The effect of the laser-induced structural transformations on mechanical properties was evaluated by studying the response of laser-treated micromechanical resonators. The Young's modulus (Y) stiffens significantly after laser annealing. These moduli were extracted from the resonant frequency of microcantilevers cut from the laser-annealed drums (with the highest Q-values) using a focused ion beam (Supporting Information, Figure S4). Figure 3D shows a plot of f^2 versus h^2/L^4 according to

$$f = A\left(\frac{Y}{\rho}\right)^{1/2}\frac{h}{L^2} \tag{2}$$

dx.doi.org/10.1021/nl3018059 | Nano Lett. 2012, 12, 4212−4218

with L = length, A = 0.162 for the fundamental mode,[30] and ρ = mass density (estimated at 2.2 g/cm^3 from Figure 3B, see Supporting Information). The slope gives a $Y = 815 \pm 14$ GPa, a remarkable 14 times increase over the starting films, despite the small sp^2-crystalline size (see Raman spectrum in Figure 3C). We emphasize the observed enhancement in stiffness applies to the in-plane Young's modulus. Although eq 2 was derived for an isotropic cantilever beam, it was shown[31] to be valid (within a few percent) for thin anisotropic plates as well, assuming the use of the in-plane Young's modulus. FEM results for the FIB-machined cantilevers (see Supporting Information) and domes in Figure 2C (calculated based on the same transversely isotropic material model) confirm this dramatic increase in in-plane stiffness.

To determine whether increased stiffness is accompanied by increased strength, the annealed drum resonators were subjected to stress relaxation experiments where the resonator stress (extracted from f_{res} at RT) was measured as a function of the anneal time, accumulated at 725 K (Figure 3E). As described earlier, resonators not laser-annealed (stars, Figure 3E) relax after 5 min and then form domes upon cooling to RT. In contrast, laser recrystallized resonators maintain a residual stress that depends on P_{laser}. The highest stress resonators (e.g., P = 1.4 mW, Figure 3E) maintained ~80% their initial stress after 120 min at 725 K, confirming increased strength with laser annealing.

In the framework of a viscoelastic model, we can compare CMG stress resilience in terms of a common activation energy (E_A) associated with platelet slippage. A one-dimensional Maxwell model (dashpot and a spring of stiffness Y_s in series[32]) predicts a decay of σ according to

$$\dot{\varepsilon} = \frac{\sigma}{M\tau_0 e^{E_A/k_B T}} + \frac{1}{Y_s}\dot{\sigma} = 0 \tag{3}$$

where ε is total strain (defined by TEC difference between graphene and silicon), the constant M and $\tau_0 \exp(E_A/k_B T)$ (the temperature dependent relaxation time) define the viscosity of the dashpot, and k_B is Boltzmann's constant. To extract relative values of E_A for laser-annealed resonators, we take the ratio of $\dot{\sigma}/\sigma$ for different films and assume Y_s is defined by the Young's modulus, leading to

$$E_{A2} = E_{A1}\frac{T_2}{T_1} + k_B T_2 \ln\left[\frac{Y_2{}^*\dot{\sigma}_1/\sigma_1}{Y_1{}^*\dot{\sigma}_2/\sigma_2}\right] \tag{4}$$

Equation 3 enables the comparison of the activation energy E_{A1} for chemically reduced CMG films ($\dot{\sigma}/\sigma$ measured in wafer-bending experiment) with E_{A2} for the laser-treated resonators with the highest Q-values. Assuming that the increase in relaxation time is caused solely by changes in activation energy and using measured values for $Y_{1,2}$ (58 GPa, 815 GPa), $T_{1,2}$ (450 K, 725 K), $\dot{\sigma}/\sigma$ (steady-state slopes at t > 200 min.), and $E_{A1} \approx 0.08$ eV for graphite,[33] we estimate $E_{A2} \approx 0.31$ eV. This represents a four times increase in the slip-stick activation energy compared to a noncross-linked microstructure.

The striking performance boost of laser-treated resonators, an enhancement in frequency (greater than five times) and quality factor (greater than twenty times), arises from the films' capacity to sustain tensile stresses up to 1 GPa (Figure 4). Tensile stress in membrane-type resonators is known to enhance Qs.[7,34] The associated increase in the effective spring constant raises the total stored energy (W_{total}) and elevates Q according to

$$Q = \frac{W_{total}}{W_{diss}} = \frac{W_{total}}{W_{diss}^{film} + W_{diss}^{clamping} + W_{diss}^{viscous}} \tag{5}$$

where W_{diss} is the energy dissipated per cycle and the superscripts are for various loss mechanisms (W^{film} includes internal friction and possible surface loss associated with the suspended film). At low laser annealing powers (P < 0.75 mW, Figure 4A,B), we observe the expected qualitative relationship, Q increases with f_{res} (Figure 4B). However, at higher powers (0.75mW < P < 1.75mW), Q increases while f_{res} decreases (arrows mark f_{max}, Figure 4B). Such an increase in Q with decreasing W_{total} can only occur by reducing W_{diss} in eq 5. Thus, the $Q \approx 31\,000$ (Figure 4C) results from engineering high residual tensile stress, as well as a refined microstructure via laser annealing.

We attribute the nonmonotonic behavior of frequency versus laser power (Figure 4A) to the balance between the volume reduction during recrystallization and platelet slippage (i.e., relaxation) activated at elevated temperatures at the laser "hot spot". Given that the activation energy for slip-stick events is affected by the extent of cross-linking (induced by recrystallization), one would expect a nonlinear dependence for the resulting tensile stress and quality factor. Understanding the recrystallization process on a microscopic level would enable further Q improvements through optimized thermal treatments. Raman spectra from the highest Q resonators consistently have the broadest D and G peaks (e.g., Figure 3C), emphasizing the needed increase in sp^3 C content to improve mechanical performance. We also note that CMG resonator Qs show a 15× increase over the highest Qs reported at RT for pristine graphene drums,[35] which illustrate the importance of mechanical tunability versus an untunable though structurally perfect starting material. We anticipate significant Q enhancement for CMG resonators at cryogenic temperatures based on the temperature dependence of the internal friction for disordered carbon.[36] A comparison of the low-temperature behavior of the dissipation in high-Q CMG resonators to pure graphene[37] can provide further insights regarding the microscopic structure and the nature of the dissipation mechanism.

Finally, Figure 4D illustrates that resonators annealed at the laser powers that provide the highest Q-values (P_{laser} = 3.3 mW in Figure 4D) show the tendency to retain the highest tensile stress after an extended, high temperature anneal (T > 1025 K). We emphasize that tensile stress in the range 500−900 MPa observed in laser-treated resonators after subsequent thermal anneal at 700 K (Figure 4D) is in sharp contrast with stress relaxation observed in multilayer graphene without cross-linking, which undergo wrinkle formation under similar thermal treatment.[21] Such enhanced resilience of CMG films is in line with the estimated four times increase in slip-stick activation energy. The highest stress, $\sigma \sim 1000$ MPa (from eq 1 using density estimated for a 1mW laser annealed resonator, see Supporting Information), demonstrated by the drum laser-annealed at 1.2 mW (Figure 4D) provides a lower-bound estimate for the CMG strength at RT and is truly remarkable for a film that started as loosely bound platelets. The actual yield stress for laser-annealed CMG films could be even higher given that experimentally determined value could be limited by the interfacial shear strength (at the clamping boundary).[16]

The transformation from a "van der Waals" solid into a three-dimensional (3D)-networked material with high stiffness and strength highlights our approach for controlling graphene's mechanical properties. The intra- and interplatelet engineering

establishes a toolbox to mold CMG into a carbon-based "nanomaterial-by-design", enabling applications from "nano-shrink wrap" and gas impermeable encapsulation to self-assembly, powered by a contracting CMG film. Implementation of such structures is greatly facilitated by the compatibility of CMG process flow with wafer-scale fabrication. Preliminary results also indicate that e-beam irradiation can be an effective method for local chemical modification, opening possibilities for mechanical tuning with nanoscale lateral resolution (see Supporting Information). Furthermore, opportunities exist to induce structural transformations in clamped (i.e., non-suspended) CMG films using pulsed lasers, a tool widely used in laser recrystallization of silicon.[38] However, detailed understanding of the microscopic mechanism for recrystallization and interplatelet cross-linking requires more theoretical and experimental effort. While Raman spectroscopy provides a good insight regarding film recrystallization, in order to build a true microscopic model we are currently preparing TEM measurements. In particular, the role of residual fluorine atoms could be vital,[39] given we were so far unable to induce similar transformations in nonfluorinated, multilayer rGO resonators.[10]

In conclusion, a combination of numerical analysis, wafer-scale measurements and the response of the lithographically defined nanomechanical structures showed the effect of adatoms and defect manipulation on the mechanical properties of multilayer graphene-based films. Low-temperature processing of CMG generates up to 400 MPa of internal stress, while laser irradiation of suspended CMG produces a 3D-networked material with improved Yield strength (≥1 GPa at RT), Young's modulus ($Y \approx 815$ GPa) and enables implementation of RF nanomechanical resonators with high quality factors ($Q \approx 31\,000$ at RT). We envision incorporating these materials in numerous applications in nanomechanics, from sensing to quantum computing elements, where tailoring the mechanics of ultrathin films is critically enabling.

Methods. Wafer bending measurements were carried out using 4 in., 100 μm thick or 3 in., 50 μm thick double-side polished Si wafers and their curvature was measured using a Veeco Dektak 150 Surface profiler. As-received wafers were oxygen plasma cleaned (2 min) and then annealed at 875K (1 h) to relax any internal stress that might change the wafer shape during subsequent heat treatments up to 725 K. GO films were then deposited from solution using spin-casting.[10] The internal stress was calculated using Stoney's Equation (see Supporting Information). We used a Digital Instruments atomic force microscope to measure both film and resonator thicknesses (Supporting Information Figure S2). To measure resonator thickness, some resonators were intentionally crashed to lie flat on the substrate. Raman spectra were acquired using confocal Raman system with a single-mode 532 nm laser and a Princeton Instruments CCD array.

The resonance frequencies of suspended drums and cantilevers were measured in vacuum ($\sim 10^{-7}$ Torr) using conventional optical techniques[5,10] with a 412 nm drive laser and a 633 nm "read out" laser. Laser irradiation was also performed in vacuum primarily with $\lambda = 532$ nm but confirmed to work at $\lambda = 633$ nm and $\lambda = 412$ nm. The laser beam ($\sim$1 μm) was rastered in a square 2D-array over the drums in 0.5 μm steps with a $\sim$0.3 s dwell time. Laser powers were measured directly outside of the vacuum chamber window. Two movies are included as additional supplementary files that demonstrate domes changing shape upon laser exposure and becoming "white-hot" at high laser powers. Cantilevers were cut from laser annealed drums with $Q > 10{,}000$ using a focused ion beam system (see Supporting Information Figure S4).

All DFT calculations where performed using Quantum Espresso version 4.1.2 on a SGI Altix 4700 machine. We used the pseudopotentials C.pbe-van_ak.UPF, F.pbe-n-van.UPF, H.pbe-van_ak.UPF, and O.pbe-van_ak.UPF from http://www.quantum-espresso.org.

■ ASSOCIATED CONTENT

Supporting Information

A detailed description of the fabrication techniques, measurement procedures and DFT analysis. This material is available free of charge via the Internet at http://pubs.acs.org.

■ AUTHOR INFORMATION

Corresponding Author

*E-mail: jeremy.robinson@nrl.navy.mil.

Present Addresses

‡NRC Postdoctoral Research Associate residing at NRL.
§Nova Research, Inc. employee residing at NRL.

Author Contributions

†These authors contributed equally to this work.

Notes

The authors declare no competing financial interest.

■ ACKNOWLEDGMENTS

The authors are grateful for funding from the Office of Naval Research and NRL's Nanoscience Institute. We thank David Zapotok and Dean St. Amand in NRL's Nanoscience Institute for continual technical support. We thank D. Photiadis, J. M. Parpia and R. Rendell for discussions.

■ REFERENCES

(1) Hussain, F.; Hojjati, M.; Okamoto, M.; Gorga, R. E. *J. Compos. Mater.* **2006**, *40* (17), 1511−1575.

(2) Park, S.; Lee, K.-S.; Bozoklu, G.; Cai, W.; Nguyen, S. T.; Ruoff, R. S. *ACS Nano* **2008**, *2* (3), 572−578.

(3) Compton, O. C.; Cranford, S. W.; Putz, K. W.; An, Z.; Brinson, L. C.; Buehler, M. J.; Nguyen, S. T. *ACS Nano* **2012**, *6* (3), 2008−2019.

(4) Ruoff, R. *Nature* **2012**, *483* (7389), S42−S42.

(5) Bunch, J. S.; van der Zande, A. M.; Verbridge, S. S.; Frank, I. W.; Tanenbaum, D. M.; Parpia, J. M.; Craighead, H. G.; McEuen, P. L. *Science* **2007**, *315* (5811), 490−493.

(6) Lee, C.; Wei, X.; Kysar, J. W.; Hone, J. *Science* **2008**, *321* (5887), 385−388.

(7) Verbridge, S. S.; Parpia, J. M.; Reichenbach, R. B.; Bellan, L. M.; Craighead, H. G. *J. Appl. Phys.* **2006**, *99* (12), 124304−8.

(8) Stankovich, S.; Dikin, D. A.; Piner, R. D.; Kohlhaas, K. A.; Kleinhammes, A.; Jia, Y.; Wu, Y.; Nguyen, S. T.; Ruoff, R. S. *Carbon* **2007**, *45* (7), 1558−1565.

(9) Elias, D. C.; Nair, R. R.; Mohiuddin, T. M. G.; Morozov, S. V.; Blake, P.; Halsall, M. P.; Ferrari, A. C.; Boukhvalov, D. W.; Katsnelson, M. I.; Geim, A. K.; Novoselov, K. S. *Science* **2009**, *323* (5914), 610−613.

(10) Robinson, J. T.; Zalalutdinov, M.; Baldwin, J. W.; Snow, E. S.; Wei, Z.; Sheehan, P.; Houston, B. H. *Nano Lett.* **2008**, *8* (10), 3441−3445.

(11) Tu, K.-N.; Mayer, J. W.; Feldman, L. C. Electronic Thin Film Science For Electrical Engineers and Material Scientists. In *Stress in Thin Film*; Macmillian Publishing Company: New York, 1992; pp 84−88.

(12) Madou, M. J. Surface Micromachining. In *Fundamentals of Microfabrication: The Science of Miniaturization*, 2nd ed.; CRC Press: Boca Raton, FL, 2002; p 301.

(13) Dikin, D. A.; Stankovich, S.; Zimney, E. J.; Piner, R. D.; Dommett, G. H. B.; Evmenenko, G.; Nguyen, S. T.; Ruoff, R. S. *Nature* **2007**, *448* (7152), 457−460.
(14) Mattevi, C.; Eda, G.; Agnoli, S.; Miller, S.; Mkhoyan, K. A.; Celik, O.; Mastrogiovanni, D.; Granozzi, G.; Garfunkel, E.; Chhowalla, M. *Adv. Funct. Mater.* **2009**, *19* (16), 2577−2583.
(15) Bagri, A.; Mattevi, C.; Acik, M.; Chabal, Y. J.; Chhowalla, M.; Shenoy, V. B. *Nature Chem.* **2010**, *2* (7), 581−587.
(16) Conley, H.; Lavrik, N. V.; Prasai, D.; Bolotin, K. I. *Nano Lett.* **2011**, *11* (11), 4748−4752.
(17) Giannozzi, P.; Baroni, S.; Bonini, N.; Calandra, M.; Car, R.; Cavazzoni, C.; Ceresoli, D.; Chiarotti, G. L.; Cococcioni, M.; Dabo, I.; Dal Corso, A.; Fabris, S.; Fratesi, G.; Gironcoli, S. d.; Gebauer, R.; Gerstmann, U.; Gougoussis, C.; Kokalj, A.; Lazzeri, M.; Martin-Samos, L.; Marzari, N.; Mauri, F.; Mazzarello, R.; Paolini, S.; Pasquarello, A.; Paulatto, L.; Sbraccia, C.; Scandolo, S.; Sclauzero, G.; Seitsonen, A. P.; Smogunov, A.; Umari, P.; Wentzcovitch, R. M. *J. Phys: Condens. Matter* **2009**, *21*, 395502.
(18) Suk, J. W.; Piner, R. D.; An, J.; Ruoff, R. S. *ACS Nano* **2010**, *4* (11), 6557−6564.
(19) Robinson, J. T.; Burgess, J. S.; Junkermeier, C. E.; Badescu, S. C.; Reinecke, T. L.; Perkins, F. K.; Zalalutdniov, M. K.; Baldwin, J. W.; Culbertson, J. C.; Sheehan, P. E.; Snow, E. S. *Nano Lett.* **2010**, *10* (8), 3001−3005.
(20) Finnie, I.; Heller, W. Creep of Engineeering Materials; McGraw-Hill Book Company, Inc.: New York, 1959; pp 38, 120.
(21) Bao, W.; Miao, F.; Chen, Z.; Zhang, H.; Jang, W.; Dames, C.; Lau, C. N. *Nat. Nanotechnol.* **2009**, *4* (9), 562−566.
(22) Bower, A. F. Linear Elastic Material Behavior. In *Applied Mechanics of Solids*; CRC Press: Boca Raton, FL, 2010; pp 83−86.
(23) Gomez-Navarro, C.; Meyer, J. C.; Sundaram, R. S.; Chuvilin, A.; Kurasch, S.; Burghard, M.; Kern, K.; Kaiser, U. *Nano Lett.* **2010**, *10* (4), 1144−1148.
(24) Telling, R. H.; Ewels, C. P.; El-Barbary, A. A.; Heggie, M. I. *Nat. Mater.* **2003**, *2* (5), 333−337.
(25) Kotakoski, J.; Krasheninnikov, A. V.; Kaiser, U.; Meyer, J. C. *Phys. Rev. Lett.* **2011**, *106*, 105505.
(26) Ferrari, A. C.; Meyer, J. C.; Scardaci, V.; Casiraghi, C.; Lazzeri, M.; Mauri, F.; Piscanec, S.; Jiang, D.; Novoselov, K. S.; Roth, S.; Geim, A. K. *Phys. Rev. Lett.* **2006**, *97* (18), 187401.
(27) Bauschlicher, C. W., Jr.; Lawson, J. W. *Chem. Phys.* **2010**, *374* (1−3), 77−82.
(28) Urita, K.; Suenaga, K.; Sugai, T.; Shinohara, H.; Iijima, S. *Phys. Rev. Lett.* **2005**, *94* (15), 155502.
(29) Barreiro, A.; Börrnert, F.; Rümmeli, M. H.; Büchner, B.; Vandersypen, L. M. K. *Nano Lett.* **2012**, *12* (4), 1873−1878.
(30) Morse, P. M.; Ingard, K. U. Bars, Membranes, and Plates. In *Theoretical Acoustics*; Princeton University Press: Princeton, NJ, 1968; pp 181−182.
(31) Dudek, T. J. *J. Compos. Mater.* **1970**, *4*, 232−241.
(32) Nowick, A. S.; Berry, B. S. Anelastic Relaxation in Crystalline Solids. In *Anelastic Relaxation in Crystalline Solids*; Academic Press: New York, 1972; pp 44, 58.
(33) Dienwiebel, M.; Pradeep, N.; Verhoeven, G. S.; Zandbergen, H. W.; Frenken, J. W. M. *Surf. Sci.* **2005**, *576* (1−3), 197−211.
(34) Unterreithmeier, Q. P.; Faust, T.; Kotthaus, J. P. *Phys. Rev. Lett.* **2010**, *105* (2), 027205.
(35) Barton, R. A.; Ilic, B.; van der Zande, A. M.; Whitney, W. S.; McEuen, P. L.; Parpia, J. M.; Craighead, H. G. *Nano Lett.* **2011**, *11* (3), 1232−1236.
(36) Liu, X.; Metcalf, T. H.; Mosaner, P.; Miotello, A. *Appl. Surf. Sci.* **2007**, *253* (15), 6480−6486.
(37) Eichler, A.; Moser, J.; Chaste, J.; Zdrojek, M.; Wilson Rae, I.; Bachtold, A. *Nat Nano* **2011**, *6* (6), 339−342.
(38) Thompson, M. O.; Galvin, G. J.; Mayer, J. W.; Peercy, P. S.; Poate, J. M.; Jacobson, D. C.; Cullis, A. G.; Chew, N. G. *Phys. Rev. Lett.* **1984**, *52* (26), 2360−2363.
(39) Sivek, J.; Leenaerts, O.; Partoens, B.; Peeters, F. arXiv:1109.4050v3, 2011.